

Catalysis Science & Technology

Accepted Manuscript



This is an *Accepted Manuscript*, which has been through the Royal Society of Chemistry peer review process and has been accepted for publication.

Accepted Manuscripts are published online shortly after acceptance, before technical editing, formatting and proof reading. Using this free service, authors can make their results available to the community, in citable form, before we publish the edited article. We will replace this *Accepted Manuscript* with the edited and formatted *Advance Article* as soon as it is available.

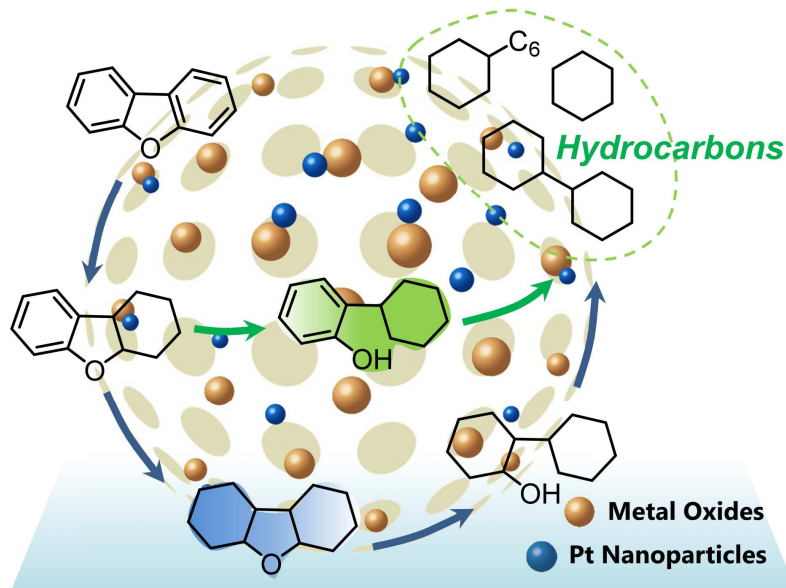
You can find more information about *Accepted Manuscripts* in the [Information for Authors](#).

Please note that technical editing may introduce minor changes to the text and/or graphics, which may alter content. The journal's standard [Terms & Conditions](#) and the [Ethical guidelines](#) still apply. In no event shall the Royal Society of Chemistry be held responsible for any errors or omissions in this *Accepted Manuscript* or any consequences arising from the use of any information it contains.

Graphic Abstract

Hydrodeoxygenation of dibenzofuran over SiO_2 , $\text{Al}_2\text{O}_3/\text{SiO}_2$ and $\text{ZrO}_2/\text{SiO}_2$ supported Pt catalysts

Lei Wang, Huihui Wan, Shaohua Jin, Xiao Chen, Chuang Li, and Changhai Liang



Highly dispersed platinum nanoparticles are supported on the Al_2O_3 or ZrO_2 modified silica for hydrodeoxygenation of dibenzofuran.

Cite this: DOI: 10.1039/c0xx00000x

www.rsc.org/xxxxxx

ARTICLE TYPE

Hydrodeoxygenation of dibenzofuran over SiO₂, Al₂O₃/SiO₂ and ZrO₂/SiO₂ supported Pt catalysts

Lei Wang, Huihui Wan, Shaohua Jin, Xiao Chen, Chuang Li, and Changhai Liang*

Received (in XXX, XXX) Xth XXXXXXXXXX 20XX, Accepted Xth XXXXXXXXXX 20XX

DOI: 10.1039/b000000x

The surface of silica with mesopores (SiO₂) was post-modified by the deposition of highly dispersed Al₂O₃ or ZrO₂ oxides. Loading of Pt on the modified silica supports yielded higher metal dispersion with respect to parent silica based on the CO chemisorption and transmission electron microscopy results. Hydrodeoxygenation (HDO) of dibenzofuran (DBF) over the as-prepared Pt catalysts mainly undergoes the hydrogenation of the aromatic rings, which is followed by the cleavage of C-O bond to produce oxygen-free hydrocarbons. Preferable hydrogenation of aromatic rings is observed over the smaller Pt nanoparticles. The relatively strong acidic properties of Al₂O₃/SiO₂ or ZrO₂/SiO₂ revealed by the NH₃-TPD profiles promote the selective C-O bond cleavage of hexahydrodibenzofuran to alert the HDO reaction pathway. The small sized Pt nanoparticles supported on the Al₂O₃ or ZrO₂ modified silica supports show superior HDO performance with enhanced deoxygenation ability to those over unmodified silica. According to the pseudo-first-ordered kinetics analysis, the fitting HDO rate constant follows the order: Pt/Al₂O₃/SiO₂>Pt/ZrO₂/SiO₂>Pt/SiO₂ under a constant temperature, which is attributed to the cooperative function of dispersed metal particles and acidic sites of supports.

1 Introduction

Currently, there is an increasing demand for renewable energy production due to the rapid energy consumption and world climate change. Renewable energy from biomass transformation is of major interest to reduce the dependence to the traditional fossil fuels.¹⁻³ The composition of these bio-oils derived from biomass includes phenols, furans, organic acids, ketones, aldehydes, *etc.*⁴ As we expected, the bio-oils contain high oxygen content, which results in high viscosity, low heating value, and poor thermal stability.⁵ There is still much upgrading work to be done before practical use of these bio-oils.

Catalytic HDO is such an alternative process to upgrade the bio-oils to hydrocarbon fuels as reported in many literatures.⁶⁻⁸ Oxygen can be removed by cleavage of C-O bond to produce water as byproduct. The HDO process is usually operated under high pressure of hydrogen and moderate temperatures, which is also applicable to the conventional hydrodesulfurization (HDS), hydrodenitrogenation (HDN), and hydrodemetallization (HDM).⁹ Furan compound is reported as a typical kind of biomass derived molecules to test the catalyst activities in the HDO reactions.^{6, 10} DBF with furan structure is considered as a lignin model compound containing the β-5 linkage which is often found in a five-membered ring linking two aromatic structures via both a C-C bond and a C-O bond.¹¹ Meanwhile, DBF is formed as an important intermediate in the biomass gasification with a weight percent of 13.19%, which is almost twice as much as another kind of major products benzene (7.13%).¹² In the past years, several groups reported the HDO of benzofuran (claimed as

another typical β-5 linkage model) or DBF as a model to study the conversion of the β-5 linkage in lignin.¹³⁻¹⁶ For the relatively larger molecular size and lower reactivity than benzofuran, the HDO of DBF as a β-5 linkage model allows determination of catalytic selectivity toward either aromatic ring hydrogenation or ether linkage cleavage.^{4, 16-18} The HDO product selectivity is closely related to the ability of hydrogenation by active metal sites and cleavage of C-O bond promoted by acidic sites in the HDO reactions.

For the rational design of HDO catalysts, the right choice of support is very important. In the last decades, zeolites,^{19, 20} silica,^{21, 22} carbon,²³ and metal oxides^{11, 24-26} have been demonstrated to be applicable as supports of HDO catalysts. Previously, metal oxides, such as Al₂O₃, ZrO₂, TiO₂, *et al.*, show good stability in the HDO reactions in the presence of water.^{27, 28} Metal catalysts supported over the metal oxides usually show enhanced metal dispersion.²⁹ It is claimed that metal oxides could activate the phenolic compounds and influence their adsorption modes in the HDO reactions, which leads to a better selectivity toward the target HDO products.^{30, 31} However, metal oxides commonly have small surface area, therefore the adsorption and concentration of reactants around the active sites is very limited. For this reason, the synthesis of mesoporous materials supported metal oxides has been investigated as an efficient way to make up for the referred deficiency.³² Deposition of metal oxides onto supports with a large surface area (i.e. ordered mesoporous silica) not only takes advantage of mesoporous materials with specific surface area and pore volume, but also exhibit properties not found in the bulk metal oxides alone.^{33, 34} For instance, Al₂O₃,

ZrO₂ or TiO₂ nanocrystalline was embedded inside the pores of SBA-15. The incorporation of metal oxides enhances the interaction of the support with NiMo catalysts with better dispersion of the active phase and improves its catalytic performance in the HDS of dibenzothiophene and its derivatives.^{35, 36}

In the present work, we modified the surface of silica with mesopores by the deposition of metal oxides Al₂O₃ or ZrO₂ to prepare a series of novel supported Pt catalysts. It is apparent that the deposited metal oxides on the surface of silica promoted the dispersion of Pt nanoparticles. The catalytic performance of such Pt/Al₂O₃/SiO₂, Pt/ZrO₂/SiO₂, and Pt/SiO₂ catalysts in the HDO of DBF was investigated to reveal the influence of support on the HDO reaction network and kinetics. The superior hydrogenation and deoxygenation ability of Pt/Al₂O₃/SiO₂ and Pt/ZrO₂/SiO₂ catalysts was attributed to both the more dispersed metal Pt particles and the unique acidic properties of the supports.

2 Experimental

2.1 Catalyst preparation

The surface of silica with mesopores was post-modified by the coating of alumina or zirconia to obtain Al₂O₃/SiO₂ or ZrO₂/SiO₂ supports according to the NH₃/water vapor-induced internal hydrolysis method.³⁷⁻³⁹ All the supports were calcined under static air at 773 K in furnace before further use. A supported catalyst with nominal 0.50 wt% Pt loading was prepared by the following steps. First, a certain amount of metal precursor H₂PtCl₆·6H₂O was dissolved in 70 mL methanol at room temperature, then 1.00 g calcined support was added under vigorously stirring until the formation of homogenous slurry. The slurry was attached to a rotary evaporator, using the bath to maintain the flask at 308 K. Methanol was removed after 30 min and the slightly damp powder was allowed to air dry at 333 K for 6 h prior to reduction. At last, the prepared catalysts were heated to 673 K at a rate of 2 K min⁻¹ and reduced for 2 h under 40 mL min⁻¹ H₂.

2.2 Catalyst characterization

X-ray diffraction (XRD) analysis of the samples was carried out using a Rigaku D/Max-RB diffractometer with Cu K α monochromatized radiation source ($\lambda=1.54178$ Å), operated at 40 KV and 100 mA. Raman measurements were obtained by a Thermo Scientific DXR Raman Microscope with a 532 nm Ar laser. The elemental contents of the catalysts, including the metal Al or Zr in the oxides and precious metal Pt, were detected either by Perkin-Elmer Optima 2000DV inductively coupled plasma atomic emission spectroscopy (ICP-AES), SRS-3400 Sequential X-ray Spectrometer System (XRF) or FEI QUANTA 450 with Energy Dispersive Spectrometer (EDS). Transmission electron microscopy (TEM) images were taken on FEI Tecnai G20 at an acceleration voltage of 300 kV.

In the case of temperature programmed desorption of ammonia (NH₃-TPD) experiments, the calcined supports were outgassed in He at 573 K for 2 h, and then saturated at 373 K in a 10% NH₃/He stream (50 mL min⁻¹) for 1 h. After removing most weakly physisorbed NH₃ by flowing He (50 mL min⁻¹), the chemisorbed NH₃ was determined with TCD detector by heating at 10 K min⁻¹ up to 973 K under the same flow of He.

Nitrogen adsorption and desorption isotherms at 77 K were measured by using Autosorb IQ surface area and pore size analyser. The specific surface area was calculated by BET (Brunauer-Emmett-Teller) method and pore volume was calculated from the volume of liquid nitrogen at p/p₀=0.99. Non-local density functional theory (NLDFT) method considering sorption of nitrogen at 77 K in cylindrical silica pores was used to determine the pore size distribution by using the adsorption branch.

CO chemisorption analysis was performed in the same Autosorb IQ apparatus under static volumetric conditions. Prior to measurement, the ex situ reduced catalysts were activated in situ in H₂ at 573 K for 2 h and evacuated for 2 h, then the furnace was cooled to 303 K. The chemisorption isotherms were obtained by measuring the amount of CO adsorbed for pressures varying from 80 to 560 mmHg at 303 K. After completing the initial analysis, the reversibly adsorbed gas was evacuated and the analysis repeated to determine the chemisorbed molecules alone. A stoichiometry CO/Metal=1 was accordingly taken to estimate the number of metal active sites.

2.3 Catalytic tests

Typically, the HDO of DBF experiments were performed at 553 K and 3.0 MPa total pressure in a continuous-flow fixed-bed reactor over 50 mg catalyst diluted with 5.0 mL 60-80 mesh quartz sands. Before the HDO experiments, the as-prepared Pt catalysts were activated in situ with 40 mL min⁻¹ H₂ at 3.0 MPa and 573 K for 1 h. Then the temperature was adjusted to the reaction temperature. The liquid reactants composed of 3.0 wt% DBF, 1.0 wt% n-dodecane (as internal standard for gas chromatography (GC) analysis), and 96.0 wt% n-decane (as inert solvent). The experimental data were collected at different weight time until the fresh catalyst reached steady state. The weight time is defined as $\tau=W_{\text{cat}}/n_{\text{feed}}$, where W_{cat} denotes the catalyst weight and n_{feed} denotes the total molar flow feed to the reactor. The varying of weight time is achieved by changing either the flow rate of liquid reactants or catalyst weight. The reaction products after being condensed in a trap at room temperature were collected and analyzed using an Agilent GC 7890A with a flame ionization detector and a 0.25 $\mu\text{m} \times 0.32\text{mm} \times 30$ m HP-5 capillary column. Product identifications were conducted on an Agilent 6890N with 5973 MSD and a 0.25 $\mu\text{m} \times 0.32\text{mm} \times 30$ m HP-5MS capillary column.

The conversion (X) and selectivity (S) in the HDO of DBF were used to present the activities of as-prepared Pt catalysts, which were calculated as

$$X=(n_0-n_{\text{DBF}})/n_0 \times 100\% \quad (1)$$

$$S=n_i/\sum n_i \times 100\% \quad (2)$$

where n_0 and n_{DBF} are the number of molecules of DBF in the feed and product, whereas n_i represents the number of molecules of a defined HDO product and $\sum n_i$ are the total number of molecules of HDO products. Turnover frequency values were calculated from the formula

$$\text{TOF}=(F/W) \times X/M \quad (3)$$

where F is the molar flow rate of reactant, W is the catalyst weight and M is the mole of active sites.

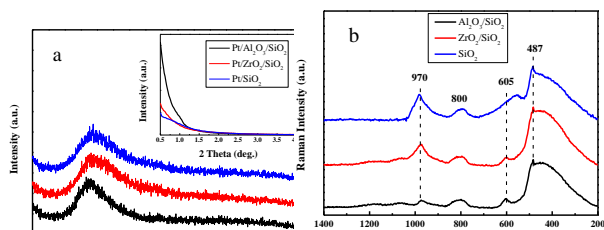


Fig. 1 Small-angle (insert) and wide-angle XRD patterns (a) of Pt/Al₂O₃/SiO₂, Pt/ZrO₂/SiO₂, and Pt/SiO₂ catalysts with 0.50 wt% Pt loading. (b) Raman spectra of Al₂O₃/SiO₂, ZrO₂/SiO₂, and SiO₂ supports using 532 nm excitation energy.

3 Results and discussion

3.1 Characterization of supports and as-prepared Pt catalysts

The surface of silica with mesopores was post-synthesis modified by the deposition of Al₂O₃ or ZrO₂ species. From the wide-angle XRD patterns in Fig. 1a, it is apparent that the surface modified samples Al₂O₃/SiO₂ or ZrO₂/SiO₂ do not exhibit any distinct peaks associated with metal oxides as compared to the original SiO₂ support. After loading of 0.50 wt% Pt on the supports, no clear Pt peaks around 2θ=40° are shown in the wide-angle XRD patterns. This is ascribed to either the quite small loaded Pt nanoparticles or the low metal loading. The small-angle XRD patterns in Fig. 1a insert are flat without typical diffraction peaks related to the ordered mesoporous structure of SiO₂. The Raman spectra of supported Al₂O₃/SiO₂ and ZrO₂/SiO₂ samples are presented in Fig. 1b and scarcely exhibit any new significant spectral features with respect to the parent SiO₂. The deposition of alumina or zirconia on the silica support causes a decrease in the intensity of the band at 970 cm⁻¹ of the Si-OH vibration, which indicates the consumption of the surface Si-OH groups.⁴⁰ The post-synthesis modification of SiO₂ surface by deposited metal oxides leads to direct interaction with the silica surface hydroxyl groups, resulting in the broadening of the 970 cm⁻¹ band. Therefore, the Al₂O₃ and ZrO₂ oxides anchor to the silica at the Si-OH site to create a surface metal oxides layer with residual exposed Si-OH species present.

In Fig. 2a, the typical type IV nitrogen adsorption-desorption isotherms of adopted supports indicate the porous structure of SiO₂ preserved after deposition of ZrO₂ or Al₂O₃ species over the surface. The BET surface areas, pore volumes, and average pore diameters are summarized in Table 1. It is obvious that the BET surface areas and pore volumes decrease sharply after deposition of metal oxides, from 405 to 221 m² g⁻¹ and 1.01 to 0.78 cm³ g⁻¹, respectively. A relatively broad pore size distribution with a pore diameter around 11.6 nm is observed from Fig. 2b. The decrease of surface areas and expansion of pore diameter (8.1 nm vs. 11.6 nm) is mostly regarded to the slight etching of surface silica by ammonium hydroxide during the post-synthesis modification. The elemental analysis by XRF and EDS confirms the successful grafting of metal oxides to the silica surface with an ideal amount. The actual amount of supported metal oxides on the SiO₂ largely exceeds the nominal loaded 0.50 wt% Pt, which is believed to be helpful for the dispersion of Pt particles.⁴² The acidity of studied supports was determined by NH₃-TPD and the desorption profiles are shown in Fig. 3. All the three supports exhibit similar TPD

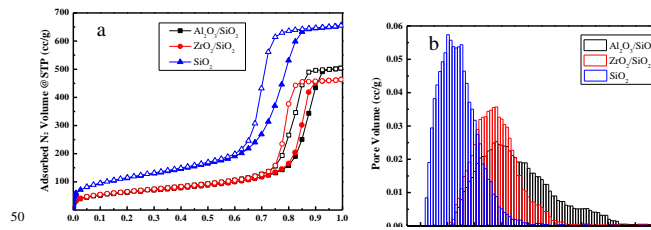


Fig. 2 Nitrogen adsorption-desorption isotherms (a) and pore size distributions (b) of Al₂O₃/SiO₂, ZrO₂/SiO₂, and SiO₂ supports.

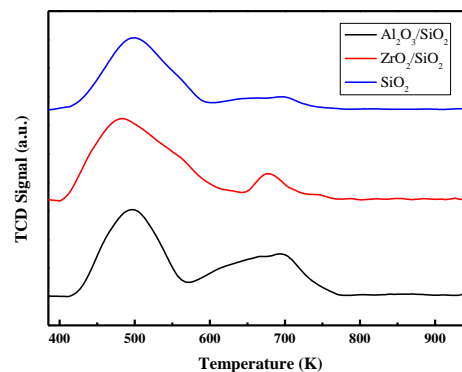


Fig. 3 NH₃-TPD profiles of the Al₂O₃/SiO₂, ZrO₂/SiO₂, and SiO₂ supports.

Table 1 Relevant physicochemical parameters of the studied supports.

Sample	S_{BET}^a (m ² g ⁻¹)	V_p^a (cm ³ g ⁻¹)	d_p^a (nm)	Metal composition ^b (wt%)	
				XRF	EDS
Al ₂ O ₃ /SiO ₂	221	0.78	11.6	1.75	1.26
ZrO ₂ /SiO ₂	224	0.72	11.6	5.47	3.76
SiO ₂	405	1.01	8.1	—	—

^a BET surface area (S_{BET}), pore volume (V_p), and average pore diameter (d_p).

^b The weight percent of Al or Zr in the modified SiO₂ supports.

profiles with two main broad peaks centered around 500 K and 700 K. These two peaks could be associated with weak acidic sites and strong acidic sites.^{24, 43} With regard to the TPD peaks, it is clear that the total acidity of the supports decreases with the order: Al₂O₃/SiO₂ > ZrO₂/SiO₂ > SiO₂, which coincides well with those previous works.²⁴

Fig. 4 displays the TEM images together with histograms of particle size of the reduced Pt catalysts. The Pt nanoparticles are highly dispersed with no apparent aggregation observed. The size of Pt nanoparticles from statistical analysis is centered at 2.5, 2.3, and 4.5 nm for the Pt/Al₂O₃/SiO₂, Pt/ZrO₂/SiO₂, and Pt/SiO₂, respectively. It is clear that the supported metal oxides Al₂O₃ or ZrO₂ promote the dispersion of Pt nanoparticles during the impregnation. The metal dispersion and Pt particle size were also estimated from the CO chemisorption and the corresponding results are listed in Table 2. Both the Pt/Al₂O₃/SiO₂ and Pt/ZrO₂/SiO₂ catalysts show more than twice the amount of CO uptake as much as Pt/SiO₂. The calculated Pt dispersion for the Pt/Al₂O₃/SiO₂ or Pt/ZrO₂/SiO₂ catalyst reaches 44% with respect to 21% for the Pt/SiO₂ catalyst. Pt particle size measured from CO chemisorption shows a good agreement with those statistical results from TEM images. The actual Pt content in the as-prepared Pt catalysts was measured by ICP-AES. All the catalysts

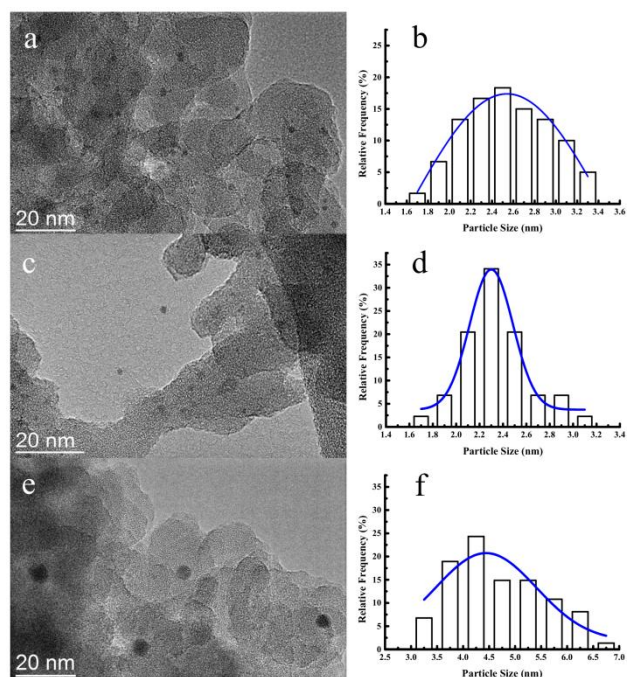


Fig. 4 TEM images and the corresponding Pt particle size distribution of Pt/Al₂O₃/SiO₂ (a, b), Pt/ZrO₂/SiO₂ (c, d), and Pt/SiO₂ (e, f) catalysts.

Table 2 CO chemisorption results of the as-prepared Pt catalysts.

Sample	CO uptake (μmol g ⁻¹)	Pt dispersion ^a (%)	Pt size (nm)
Pt/Al ₂ O ₃ /SiO ₂	11.2	44	2.6
Pt/ZrO ₂ /SiO ₂	11.3	44	2.6
Pt/SiO ₂	5.3	21	5.4

^a Estimated by assuming CO/Metal=1.

actually contained at least 0.41 wt% Pt, which is slightly less than the nominal 0.50 wt% Pt loading. Hence, the difference of Pt particle size over the studied catalysts is hardly due to the amount of metal loading. It is strongly suggested that the Al₂O₃ and ZrO₂ particles coated on the surface of SiO₂ has a positive effect on the dispersion of Pt nanoparticles during the catalyst preparation. As explained by most previous works, the metal oxides support would interact strongly with precious metal such as platinum at an elevated temperature under hydrogen.^{44, 45} The strong interaction between platinum and metal oxides suppresses the migration and aggregation of Pt nanoparticles on the surface of metal oxides.⁴¹ Therefore, the Pt catalysts impregnated on the Al₂O₃/SiO₂ or ZrO₂/SiO₂ surface show higher metal dispersion than those on the unmodified SiO₂ surface.

3.2 Product distribution of HDO over the as-prepared Pt catalysts

HDO of DBF over the as-prepared Pt/Al₂O₃/SiO₂, Pt/ZrO₂/SiO₂ and Pt/SiO₂ catalysts goes through the hydrogenation reaction route as shown in the proposed HDO reaction network (Scheme 1). Briefly, hydrogenation of aromatic rings of DBF takes first, and then oxygen removal is conducted by hydrogenolysis or dehydration/hydrogenation of saturated C-O bond to obtain bicyclohexane (BCH) and its isomer cyclopentylmethylcyclohexane (iso-BCH). Trace single-ring

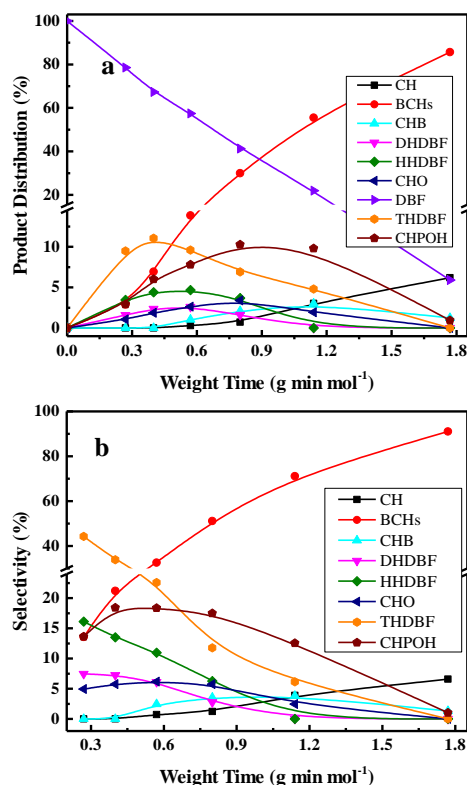


Fig. 5 Product distributions (a) and selectivities (b) of HDO of DBF over 0.50 wt% Pt/Al₂O₃/SiO₂ as a function of weight time under 280 °C and 3.0 MPa total pressure.

product cyclohexane (CH) and ring-opening products are detected as the further cracking of those bicyclo-hydrocarbons. The formation of these products and intermediates were discussed in the literature before.^{4, 17, 46}

Fig. 5 shows the HDO product distribution and selectivity over Pt/Al₂O₃/SiO₂ as a function of weight time under 280 °C and 3.0 MPa total pressure. Several main products in the HDO reaction of DBF are chosen to reveal the overall HDO reaction process. Tetrahydrodibenzofuran (THDBF), hexahydrodibenzofuran (HHDBF), and dodecahydrodibenzofuran (DHDBF) are obtained by partial or total hydrogenation of the aromatic rings of DBF. Hydrogenolysis of C-O bond of HHDBF directly produces 2-cyclohexylphenol (CHPOH). The cleavage of saturated C-O bond of DHDBF results in the production of 2-cyclohexylcyclohexanol (CHCHOH). The abbreviation CHO is defined as the sum of CHCHO and CHCHOH in the HDO products. The deoxygenation of CHPOH or CHCHOH leads to the production of BCH and iso-BCH. Finally, the C-C bond scission of these bicyclo-hydrocarbons takes place to produce small amounts of CH. Besides, the hydrogenolysis of phenolic hydroxyl in CHPOH results in CHB. At low weight time stages (e.g. 0.40 g min⁻¹), the reactant DBF mainly transforms to THDBF and HHDBF through partial hydrogenation of single aromatic ring of the DBF molecule. Less than 10% product distribution is achieved for the both THDBF and HHDBF. With increasing the weight time to 0.80 g min⁻¹, CHPOH and THDBF take more percent in the product distribution with a value close to 10%. Further hydrogenation of THDBF to HHDBF becomes preferable to

Scheme 1 Proposed reaction network of HDO of DBF over the as-prepared Pt catalysts.

result in reduced product distribution of THDBF. However, the hydrogenolysis of saturated C-O bond in the HHDBF leads to much oxygen-containing intermediates CHPOH with 11% product distribution and 18% selectivity. As the weight time increased, it is noticeable that totally deoxygenated products BCHs (BCH and iso-BCH), with BCH taking more than 90% percent, are the dominated species in the product distribution. The selectivity toward BCHs exceeds 70% at weight time higher than 1.14 g min mol⁻¹. Meanwhile, CH with measurable amount at weight time higher than 0.57 g min mol⁻¹ is explained as the further cracking of BCHs. In the whole HDO process over Pt/Al₂O₃/SiO₂, DHDBF, CHO, and CHB are detected as a small amount of products with around 2% product distribution and less than 5% selectivity in this study. The CHCHE and ring-opening products are confirmed by the GC-MS instrument with trace amount. Pt/ZrO₂/SiO₂ and Pt/SiO₂ catalysts were also tested in the HDO of DBF under the same reaction conditions to investigate the activity and reaction network of DBF. The variation trend of product distribution and selectivity are similar to those obtained over Pt/Al₂O₃/SiO₂ catalyst with 0.50 wt% Pt loading. It is worth mentioning that C-C bond scission of BCHs scarcely occurs over the Pt/ZrO₂/SiO₂ and Pt/SiO₂ catalysts with less than 1% CH yielded at weight time 1.77 g min mol⁻¹, whereas 7% CH is obtained over the Pt/Al₂O₃/SiO₂ catalyst under the same HDO reaction conditions. This comparison implies that the acidic characters of modified SiO₂ supports introduced by the deposition of oxides promote the scission of C-C bond in the help of metal active sites under such conditions. However, CH is hardly detected under the selected low weight time stages over the as-prepared Pt catalysts in this work. It is ascribed to either the relatively weak acidic properties of modified supports with limited hydrocracking ability or the short contact between the catalyst and the deoxygenated BCHs species.

3.3 Comparison of HDO over the as-prepared Pt catalysts

In order to further reveal the HDO performance of the prepared Pt catalysts, the deoxygenation degree in HDO of DBF is compared at varied HDO conversions. From Fig. 6a, it is clear that the totally deoxygenated products accumulate rapidly with increasing the HDO conversion. Hydrogenation of aromatic rings of DBF contributes more under lower HDO conversion (i.e. <40%). However, deoxygenation of the hydrogenated DBFs or the oxygen-containing compounds, cycloalcohols or cycloketones,

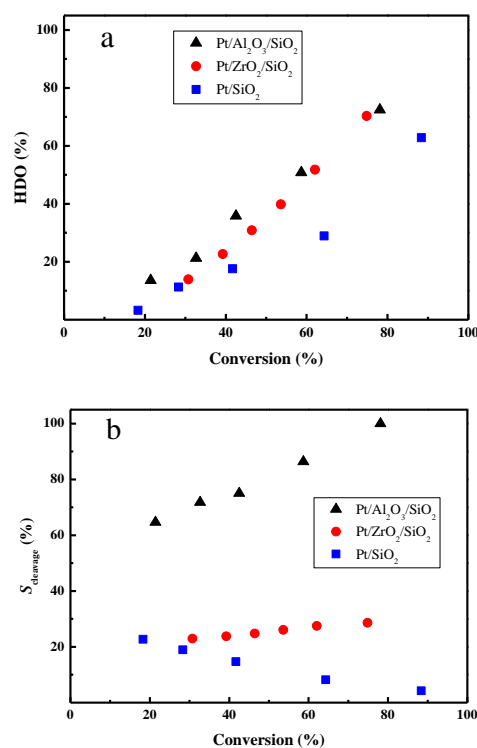


Fig. 6 The deoxygenation degree (a) and selectivity to C-O bond cleavage (b) as a function of HDO conversion under 280 °C and 3.0 MPa total pressure.

becomes favored under higher HDO conversion, which directly leads to the high yield of oxygen-free high carbon number hydrocarbon fuels. The Pt/Al₂O₃/SiO₂ and Pt/ZrO₂/SiO₂ catalysts exhibit quite similar deoxygenation abilities at high HDO conversion (>60%) stages, whereas the Pt/Al₂O₃/SiO₂ is qualified superior in deoxygenation compared with Pt/ZrO₂/SiO₂ at low conversion stages. Both the Pt/Al₂O₃/SiO₂ and Pt/ZrO₂/SiO₂ show better deoxygenation performance in comparison with Pt/SiO₂ under the studied HDO conversions.

Guided by the proposed HDO reaction network in Scheme 1, the HHDBF is either hydrogenated to DHDBF or transformed to CHPOH via hydrogenolysis of C-O bond. Hence, we calculate the selectivity to C-O bond cleavage (S_{cleavage}) with the following

formula to reveal the effect of supports to the reaction pathway.

$$S_{\text{cleavage}} = n_{\text{CHPOH}} / (n_{\text{CHPOH}} + n_{\text{DHDBF}}) \times 100\% \quad (4)$$

The S_{cleavage} for the Pt/Al₂O₃/SiO₂ catalyst with a value greater than 60% largely exceeds that for Pt/ZrO₂/SiO₂ or Pt/SiO₂ with less than 30% selectivity from Fig. 6b. With increasing the HDO conversion, the S_{cleavage} remarkable enlarges, which indicates the HHDBF mainly transforms to CHPOH with cleavage of saturated C-O bond over the Pt/Al₂O₃/SiO₂ catalyst. For the Pt/ZrO₂/SiO₂ catalyst, the calculated S_{cleavage} almost maintains the same under the varied HDO conversions. However, the gradually reduced S_{cleavage} for Pt/SiO₂ catalyst suggests that the deoxygenation of DHDBF is a major pathway in the hydrogenation reaction route. Comparing the S_{cleavage} at a given HDO conversion of 40%, it is quite apparent that more scission of saturated C-O bond takes place over the Pt/Al₂O₃/SiO₂ catalyst with a value closed to 75%. However, only 25% is obtained over the Pt/ZrO₂/SiO₂, and then 16% over the Pt/SiO₂. The obvious difference of S_{cleavage} for three studied catalysts can be mostly regarded to the varied acidic properties of the supports. The modification by Al₂O₃ or ZrO₂ changes the acidity of supports and shows a positive effect on the hydrogenolysis of the sp³ C-O bond. In the conversion of anisole and guaiacol over Pt/Al₂O₃, the hydrogenolysis of sp³ C-O bond to produce phenols and methane is kinetically significant.^{47, 48} The Ru supported on Al₂O₃ catalysts show better performance of hydrogenolysis of phenol with a preferable yield of benzene than over silica supports.⁴⁹ Over the alumina supported Pt catalysts, the vapor-phase HDO of meta-cresol produces much toluene with direct hydrogenolysis of the C-O bond.⁵⁰ Zhang *et al.* prepared a series of ZrO₂-SiO₂ supported Ni and NiCu catalysts for the hydrodeoxygenation of guaiacol.⁵¹ The hydrogenolysis of phenolic hydroxyl group with selective yield of benzene is attributed to the stronger acidity of the ZrO₂-SiO₂. These results are well consistent with this work. Regarding the mechanism of sp³ C-O bond cleavage involved in the hydrodeoxygenation of benzofuran over the sulfide catalysts, Romero *et al.* proposed that the cleavage occurs through nucleophilic substitution by a SH⁻ after protonation of the oxygen atom of 2,3-dihydrobenzofuran by a Brønsted acid site.¹³ The Al₂O₃ support contains mostly Lewis and a few Brønsted acid sites as proven by experimental and theoretical methods.^{52, 53} Whereas, the structure of C-O bond in HHDBF is similar with 2,3-dihydrobenzofuran. It is reasonable to speculate that the cleavage of C-O of HHDBF goes through similar pathway in the HDO of DBF over Pt/Al₂O₃/SiO₂. Consequently, the selective hydrogenolysis of C-O is preferable over Al₂O₃ modified SiO₂ supported Pt catalysts, while the transformation is suppressed over Pt/ZrO₂/SiO₂ and Pt/SiO₂. Besides, it is generally reported that the acidic sites of the catalysts promotes the deoxygenation of those oxygen-containing intermediates in the HDO of phenolic molecules.¹⁹ The supported Pt catalysts over the acidic zeolite HBeta show superior deoxygenation performance than Pt/SiO₂ in the HDO of anisole.²⁰ It is speculated that an acid site adjacent to a Pt particle could facilitate the deoxygenation reaction by protonating the oxygen in phenol in a bifunctional reaction. Thus, the deoxygenation of those oxygen-containing intermediates could also facilitate the hydrogenolysis of the C-O bond in the consecutive reaction of HDO, which leads to the shift of S_{cleavage} in this work.

Table 3 Comparison of HDO of DBF over the as-prepared Pt catalysts at 30% conversion.

Sample	TOF (h ⁻¹)	Selectivity (%)			
		TH+HHDBF ^a	DHDBF	OCH ^b	BCHs ^c
Pt/Al ₂ O ₃ /SiO ₂	2412	48	7	24	21
Pt/ZrO ₂ /SiO ₂	1784	56	18	12	14
Pt/SiO ₂	1678	53	24	11	12

^a The total selectivity to THDBF and HHDBFF.
^b The total selectivity to CHO and CHPOH.
^c The hydrocracking of BCHs scarcely occurs and neglect the trace CHB

The comparison of HDO reaction results at 30% conversion in Table 3 further illustrates the influence of the supports on the HDO of DBF. It is noted that the further hydrocracking of BCHs to ring-opening products and CH scarcely occurs under the studied HDO conditions. The apparent order of TOFs for the tested catalysts is as follows: Pt/Al₂O₃/SiO₂ > Pt/ZrO₂/SiO₂ > Pt/SiO₂. From the comparison of product selectivity, it is clear that the total selectivity toward THDBF and HHDBF is 48% and only 7% selectivity toward DHDBF is obtained over Pt/Al₂O₃/SiO₂ catalyst. It is particularly worth mentioning that much oxygen-containing intermediates OCH (abbreviated as the sum of CHO and CHPOH) and totally deoxygenated products BCHs are yielded with 24% and 21% selectivity, respectively. This confirms that more partially hydrogenated DBFs (THDBF and HHDBF) transform to OCH via C-O bond cleavage instead of further hydrogenation of the aromatic ring in the HDO reaction, which is consistent with those results about selectivity to C-O bond cleavage over the Pt/Al₂O₃/SiO₂ under varied conversions. The acidic properties of deposited Al₂O₃ oxides promote the cleavage of saturated C-O bond with enhanced deoxygenation performance. The Pt/ZrO₂/SiO₂ and Pt/SiO₂ catalysts showed better hydrogenation performance in the HDO of DBF with up to 70% selectivity to hydrogenated DBFs. Similar abilities of C-O bond scission are evidenced from the closed selectivity to OCH and BCHs.

The kinetic analysis of the HDO reaction was conducted at 533-573 K with varied conversions of DBF by changing the weight time. A pseudo-first-ordered model for HDO of DBF was represented by the following equation.

$$-\ln(1-X) = k_{\text{HDO}} \times \tau \quad (5)$$

The essential linear relationship of $-\ln(1-X)$ and τ is shown in Fig. 7 for the data obtained from the HDO reaction. The linear relationships illustrate that the overall reaction is pseudo-first-order. All the fitting parameters are summarized in Table 4. For instance, the HDO rate constant (k_{HDO}) over the Pt/Al₂O₃/SiO₂ catalyst increases from 0.59 to 2.03 mol g⁻¹ min⁻¹ in the temperature range from 533 to 573 K. It is obvious that the increase of temperature promotes the transformation of reactant DBF, which is quite similar with those previous works about HDO of biomass-derived molecules.³ At a constant temperature, the k_{HDO} gradually decreases following the order: Pt/Al₂O₃/SiO₂ > Pt/ZrO₂/SiO₂ > Pt/SiO₂. This phenomenon could be ascribed to the more dispersed Pt nanoparticles in the prepared

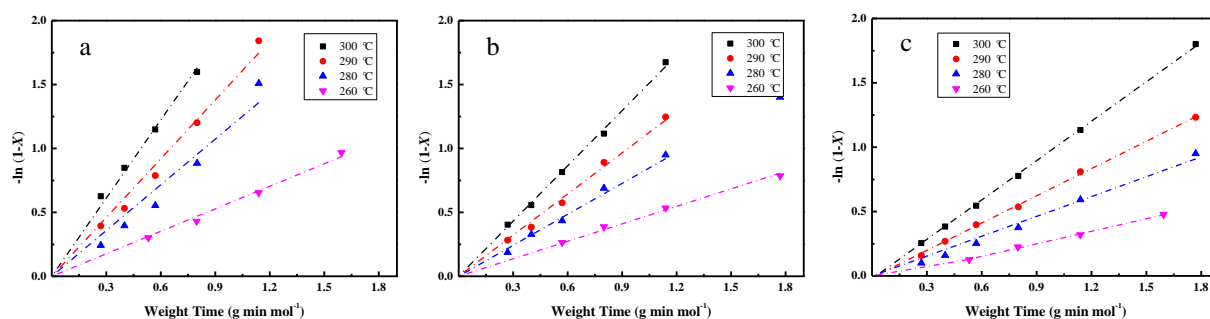


Fig. 7 Fitting of the pseudo-first-ordered kinetic model to the HDO reaction experimental data collected over Pt/Al₂O₃/SiO₂ (a), Pt/ZrO₂/SiO₂ (b), Pt/SiO₂ (c) catalysts at the temperature range from 533 to 573 K.

Table 4 Fitting parameters in the pseudo-first-ordered kinetic analysis of HDO reaction of DBF over the as-prepared Pt catalysts

Sample	HDO rate constant k_{HDO} mol g ⁻¹ min ⁻¹				r_f^a	E_a KJ mol ⁻¹	r_2^b
	573 K	563 K	553 K	533K			
Pt/Al ₂ O ₃ /SiO ₂	2.03	1.53	1.19	0.59	>0.98	79	>0.99
Pt/ZrO ₂ /SiO ₂	1.44	1.08	0.81	0.46	>0.99	72	>0.99
Pt/SiO ₂	1.01	0.71	0.51	0.32	>0.98	70	>0.98

^a The coefficient of determination in the fitting of the pseudo-first-ordered kinetic model to the HDO reaction experimental data.

^b The coefficient of determination in the linear fitting of HDO rate constant.

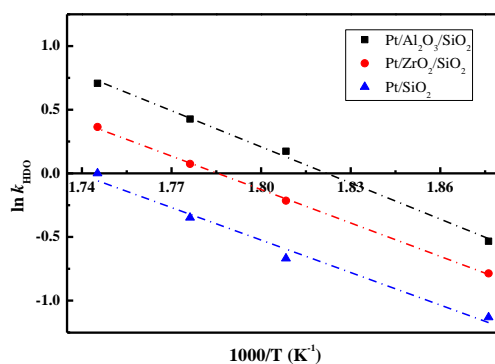


Fig. 8 HDO rate constants k_{HDO} as a function of inverse temperature.

catalysts with superior activity in the HDO of DBF. The acidic properties of supports with promotion to the deoxygenation also accelerate the transformation of DBF. Analysis of HDO rate constant-temperature dependence as shown in Fig. 8 yields HDO activation energy (E_a) with values of 79, 72, 70 KJ mol⁻¹ for the Pt/Al₂O₃/SiO₂, Pt/ZrO₂/SiO₂, and Pt/SiO₂ catalysts, respectively. Some previous works have pointed out that the catalytic HDO performance phenol conversion was obtained over smaller Pd nanoparticles in the study of hydrogenation of phenol in water.⁵⁴ In the hydrogenation of furan, small particles preferentially yielded dihydrofuran by a partial hydrogenation of the aromatic ring.⁵⁵ It is concluded that the size of supported metal nanoparticle affects the catalytic performance in the HDO of DBF. Pt nanoparticles with small size facilitate the hydrogenation of aromatic rings of DBF. As discussed from the NH₃-TPD profiles in Fig. 3, the introduction of Al₂O₃ or ZrO₂ to the surface of SiO₂ supports causes formation of stronger acid sites.

Mortensen *et al.* reported some similar results that the total acidity of the supports decreases in the following order: Ni/Al₂O₃>NiZrO₂>Ni/SiO₂.⁵⁶ The decrease of the acidity is attributed to that the low metal-oxygen bond energy with an order of $E_{(\text{Al-O})}>E_{(\text{Zr-O})}>E_{(\text{Si-O})}$ can be linked to the formation of more oxygen vacancy sites in the oxides which function as Lewis acid sites.^{57, 58} These Lewis acid sites are beneficial to the activation of the intermediates phenols via formation of phenoxide on Al₂O₃ as studied by IR spectroscopy.³⁰ The cooperative effect of support acidic sites and metal active sites has also been found to be favorable for the phenol hydrogenation on palladium catalysts, where the hydrogenation activity can be significantly increased by the introduction of Lewis acid.^{22, 59} Lee *et al.* reported the HDO of guaiacol over a series of Al₂O₃ based bifunctional catalysts. It is explained that the metal is responsible for the hydrogenation of aromatic rings and acidity appears to determine the degree of deoxygenation.⁶⁰ The ZrO₂/SiO₂ supports also have some acidic characters, but significantly less than Al₂O₃/SiO₂ supports from the NH₃-TPD results. Thus, it is still thought to have the potential to activate the oxygen-containing intermediates on its surface. Besides, the deposited Al₂O₃ oxides have a few Brønsted acid sites, which are claimed to promote the protonation of the oxygen in the HDO process. This function could further facilitate the hydrogenolysis and deoxygenation, thus accelerate the whole HDO reaction with increasing transformation of the reactant DBF. These explanations well explains the gradual change of selectivity toward deoxygenation and C-O bond cleavage in the HDO reaction over Pt/Al₂O₃/SiO₂, Pt/ZrO₂/SiO₂, and Pt/SiO₂ catalysts. The better dispersed metal particles and acidic properties of supports function cooperatively to promote the whole HDO reaction of DBF with apparently reduced HDO rate constant k_{HDO} .⁶¹

Conclusions

The deposited Al₂O₃ or ZrO₂ oxides on the surface of silica with mesopores largely help disperse Pt nanoparticles with smaller particle size. HDO of DBF over the as-prepared Pt catalysts mainly goes through the hydrogenation reaction route. Pt/Al₂O₃/SiO₂ and Pt/ZrO₂/SiO₂ catalysts with highly dispersed Pt nanoparticles show better HDO performance with superior hydrogenation activity of aromatic rings. Al₂O₃/SiO₂ and ZrO₂/SiO₂ supports with relatively strong acidic sites promote the cleavage of saturated C-O bond with enhanced deoxygenation activity in the HDO reaction. From the varied values of S_{cleavage} , it is obvious that relatively strong acidic sites of Al₂O₃/SiO₂ and ZrO₂/SiO₂ supports selectively alert the reaction pathways to CHPOH through hydrogenolysis of saturated C-O bond. However, further hydrogenation of HHDBF to DHDBF is favored over the Pt/SiO₂ catalysts with less acidic properties. A detailed analysis based on the pseudo-first-order kinetics suggests that the activity of the as-prepared Pt catalysts in the HDO reaction of DBF declines in the following order: Pt/Al₂O₃/SiO₂ > Pt/ZrO₂/SiO₂ > Pt/SiO₂. It is concluded that the smaller sized Pt nanoparticles with better hydrogenation activity and acidic properties of deposited Al₂O₃ or ZrO₂ oxides function cooperatively to the HDO of DBF with enhanced HDO performance observed.

Acknowledgements

We gratefully acknowledge the financial support provided by the National Natural Science Foundation of China (21373038) and the Fundamental Research Funds for the Central Universities (DUT12YQ03 and DUT13RC(3)41).

Notes and references

Laboratory of Advanced Materials and Catalytic Engineering, School of Chemical Engineering, Dalian University of Technology, Dalian 116012, China. Fax: +86-411-84986353; Tel: +86-411-84986353; E-mail: changhai@dlut.edu.cn

- P. Gallezot, *Chem. Soc. Rev.*, 2012, **41**, 1538-1558.
- M. Stocker, *Angew. Chem. Int. Ed.*, 2008, **47**, 9200-9211.
- D. M. Alonso, J. Q. Bond and J. A. Dumesic, *Green Chem.*, 2010, **12**, 1493.
- E. Furimsky, *Appl. Catal.*, A 2000, **199**, 147-190.
- G. W. Huber and A. Corma, *Angew. Chem. Int. Ed.*, 2007, **46**, 7184-7201.
- A. D. Sutton, F. D. Waldie, R. L. Wu, M. Schlaf, L. A. Silks and J. C. Gordon, *Nature Chem.*, 2013, **5**, 428-432.
- P. M. Mortensen, J. D. Grunwaldt, P. A. Jensen, K. G. Knudsen and A. D. Jensen, *Appl. Catal.*, A, 2011, **407**, 1-19.
- J. S. Yoon, Y. Lee, J. Ryu, Y. A. Kim, E. D. Park, J. W. Choi, J. M. Ha, D. J. Suh and H. Lee, *Appl. Catal.*, B, 2013, **142**, 668-676.
- B. Dhandapani, T. St. Clair and S. T. Oyama, *Appl. Catal.*, A, 1998, **168**, 219-228.
- S. Sitthisa and D. E. Resasco, *Catal. Lett.*, 2011, **141**, 784-791.
- J. Zakzeski, P. C. A. Bruijninx, A. L. Jongerius and B. M. Weckhuysen, *Chem. Rev.*, 2010, **110**, 3552-3599.
- C. M. Huelsman and P. E. Savage, *Phys. Chem. Chem. Phys.*, 2012, **14**, 2900-2910.
- Y. Romero, F. Richard, Y. Renème and S. Brunet, *Appl. Catal.*, A 2009, **353**, 46-53.
- A. Y. Bunch and U. S. Ozkan, *J. Catal.*, 2002, **206**, 177-187.
- Y. X. Wang, Y. M. Fang, T. He, H. Q. Hu and J. H. Wu, *Catal. Commun.*, 2011, **12**, 1201-1205.
- J. A. Cecilia, A. Infantes-Molina, E. Rodriguez-Castellon, A. Jimenez-Lopez and S. T. Oyama, *Appl. Catal.*, B, 2013, **136**, 140-149.
- L. Wang, M. M. Zhang, M. Zhang, G. Y. Sha and C. H. Liang, *Energy Fuels*, 2013, **27**, 2209-2217.
- V. Lavopa and C. N. Satterfield, *Energy Fuels*, 1987, **1**, 323-331.
- D. Y. Hong, S. J. Miller, P. K. Agrawal and C. W. Jones, *Chem. Commun.*, 2010, **46**, 1038-1040.
- X. L. Zhu, L. L. Lobban, R. G. Mallinson and D. E. Resasco, *J. Catal.*, 2011, **281**, 21-29.
- R. Nava, B. Pawelec, P. Castano, M. C. Alvarez-Galvan, C. V. Loricera and J. L. G. Fierro, *Appl. Catal.*, B, 2009, **92**, 154-167.
- C. Zhao, Y. Kou, A. A. Lemonidou, X. B. Li and J. A. Lercher, *Chem. Commun.*, 2010, **46**, 412-414.
- H. Liu, T. Jiang, B. Han, S. Liang and Y. Zhou, *Science*, 2009, **326**, 1250-1252.
- Y. Yang, C. Ochoa-Hernández, V. A. de la Peña O'Shea, P. Pizarro, J. M. Coronado and D. P. Serrano, *Appl. Catal.*, B, 2014, **145**, 91-100.
- S. K. Maity, M. S. Rana, B. N. Srinivas, S. K. Bej, G. M. Dhar and T. S. R. P. Rao, *J. Mol. Catal. A: Chem.*, 2000, **153**, 121-127.
- T. Nimmanwudipong, C. Aydin, J. Lu, R. C. Runnebaum, K. C. Brodwater, N. D. Browning, D. E. Block and B. C. Gates, *Catal. Lett.*, 2012, **142**, 1190-1196.
- A. L. Jongerius, J. R. Copeland, G. S. Foo, J. P. Hofmann, P. C. A. Bruijninx, C. Sievers and B. M. Weckhuysen, *ACS Catal.*, 2013, **3**, 464-473.
- A. L. Jongerius, P. C. A. Bruijninx and B. M. Weckhuysen, *Green Chem.*, 2013, **15**, 3049.
- A. Villa, M. Schiavoni and L. Prati, *Catal. Sci. Technol.*, 2012, **2**, 673-682.
- A. Popov, E. Kondratieva, J. M. Goupil, L. Marley, P. Bazin, J. P. Gilson, A. Travert and F. Mauge, *J. Phys. Chem. C*, 2010, **114**, 15661-15670.
- V. A. Yakovlev, S. A. Khromova, O. V. Sherstyuk, V. O. Dundich, D. Y. Ermakov, V. M. Novopashina, M. Y. Lebedev, O. Bulavchenko and V. N. Parmon, *Catal. Today*, 2009, **144**, 362-366.
- H. Gies, S. Grabowski, M. Bandyopadhyay, W. Grunert, O. P. Tkachenko, K. V. Klementiev and A. Birkner, *Microporous Mesoporous Mater.*, 2003, **60**, 31-42.
- J. Strunk, W. C. Vining and A. T. Bell, *J. Phys. Chem. C*, 2011, **115**, 4114-4126.
- P. Kustrowski, L. Chmielarz, R. Dziembaj, P. Cool and E. F. Vansant, *J. Phys. Chem. B*, 2005, **109**, 11552-11558.
- T. Klimova, L. Pena, L. Lizama, C. Salcedo and O. Y. Gutierrez, *Ind. Eng. Chem. Res.*, 2009, **48**, 1126-1133.
- O. Y. Gutierrez, D. Valencia, G. A. Fuentes and T. Klimova, *J. Catal.*, 2007, **249**, 140-153.
- H. Wan, J. Yan, L. Yu, X. Zhang, X. Xue, X. Li and X. Liang, *Talanta*, 2010, **82**, 1701-1707.
- C. K. Krishnan, T. Hayashi, and M. Ogura, *Adv. Mater.*, 2008, **20**, 2131-2136.
- C. K. Krishnan, T. Hayashi, and M. Ogura, *Microporous Mesoporous Mater.*, 2008, **116**, 406-414.
- X. T. Gao and I. E. Wachs, *J. Catal.*, 2000, **192**, 18-28.
- X. T. Gao, J. L. G. Fierro and I. E. Wachs, *Langmuir*, 1999, **15**, 3169-3178.
- Y. Nagai, T. Hirabayashi, K. Dohmae, N. Takagi, T. Minami, H. Shinjoh and S. Matsumoto, *J. Catal.*, 2006, **242**, 103-109.
- S. H. Jin, Z. H. Xiao, C. Li, X. Chen, L. Wang, J. C. Xing, W. Z. Li and C. H. Liang, *Catal. Today*, 2014, **234**, 125-132.
- S. J. Tauster and S. C. Fung, *J. Catal.*, 1978, **55**, 29-35.
- S. J. Tauster, S. C. Fung and R. L. Garten, *J. Am. Chem. Soc.*, 1978, **100**, 170-175.
- M. J. Girgis and B. C. Gates, *Ind. Eng. Chem. Res.*, 1994, **33**, 2301-2313.
- R. C. Runnebaum, R. J. Lobo-Lapidus, T. Nimmanwudipong, D. E. Block and B. C. Gates, *Energy Fuels*, 2011, **25**, 4776-4785.
- T. Nimmanwudipong, R. C. Runnebaum, D. E. Block and B. C. Gates, *Energy Fuels*, 2011, **25**, 3417-3427.
- C. Newman, X. Zhou, B. Goundie, I. T. Ghampson, R. A. Pollock, Z. Ross, M. C. Wheeler, R. W. Meulenber, R. N. Austin and B. G. Frederick, *Appl. Catal.*, A 2014, **477**, 64-74.
- P. T. M. Do, A. J. Foster, J. G. Chen and R. F. Lobo, *Green Chemistry*, 2012, **14**, 1388-1397.
- X. Zhang, T. Wang, L. Ma, Q. Zhang, Y. Yu and Q. Liu, *Catal. Commun.*, 2013, **33**, 15-19.

-
52. M. Digne, P. Sautet, P. Raybaud, P. Euzen and H. Toulhoat, *J. Catal.*, 2002, **211**, 1-5.
53. S. Jongpatiwut, Z. Li, D. E. Resasco, W. E. Alvarez, E. L. Sughrue and G. W. Dodwell, *Appl. Catal., A* 2004, **262**, 241-253.
- 5 54. Z. L. Li, J. H. Liu, C. G. Xia and F. W. Li, *ACS Catal.*, 2013, **3**, 2440-2448.
55. C. J. Kliewer, C. Aliaga, M. Bieri, W. Huang, C. K. Tsung, J. B. Wood, K. Komvopoulos and G. A. Somorjai, *J. Am. Chem. Soc.*, 2010, **132**, 13088-13095.
- 10 56. P. M. Mortensen, J. D. Grunwaldt, P. A. Jensen and A. D. Jensen, *ACS Catal.*, 2013, **3**, 1774-1785.
57. D. G. Rethwisch and J. A. Dumesic, *Langmuir*, 1986, **2**, 73-79.
58. H. Idriss and M. A. Barteau, *Adv. Catal.*, 2000, **45**, 261-331.
59. J. Matos and A. Corma, *Appl. Catal., A* 2011, **404**, 103-112.
- 15 60. C. R. Lee, J. S. Yoon, Y. W. Suh, J. W. Choi, J. M. Ha, D. J. Suh and Y. K. Park, *Catal. Commun.*, 2012, **17**, 54-58.
61. A. J. Foster, P. T. M. Do and R. F. Lobo, *Top. Catal.*, 2012, **55**, 118-128.